*Exploration Geophysics (2006) **37**, 60-66*
Butsuri-Tansa (Vol. 59, No. 1)
Mulli-Tamsa (Vol. 9, No. 1)

Velocity-effective stress response of CO_2-saturated sandstones

Anthony F. Siggins

Key Words: Carbon dioxide, sequestration, pore pressure, velocity, attenuation

ABSTRACT

Three differing sandstones, two synthetic and one field sample, have been tested ultrasonically under a range of confining pressures and pore pressures representative of in-situ reservoir pressures. These sandstones include: a synthetic sandstone with calcite intergranular cement produced using the CSIRO Calcite In-situ Precipitation Process (CIPS); a synthetic sandstone with silica intergranular cement; and a core sample from the Otway Basin Waarre Formation, Boggy Creek 1 well, from the target lithology for a trial CO_2 pilot project. Initial testing was carried on the cores at "room-dried" conditions, with confining pressures up to 65 MPa in steps of 5 MPa. All cores were then flooded with CO_2, initially in the gas phase at 6 MPa, 22°C, then with liquid-phase CO_2 at a temperature of 22°C and pressures from 7 MPa to 17 MPa in steps of 5 MPa. Confining pressures varied from 10 MPa to 65 MPa. Ultrasonic waveforms for both P- and S-waves were recorded at each effective pressure increment. Velocity versus effective pressure responses were calculated from the experimental data for both P- and S-waves. Attenuations ($1/Q_p$) were calculated from the waveform data using spectral ratio methods. Theoretical calculations of velocity as a function of effective pressure for each sandstone were made using the CO_2 pressure-density and CO_2 bulk modulus-pressure phase diagrams and Gassmann effective medium theory.

Flooding the cores with gaseous phase CO_2 produced negligible change in velocity-effective stress relationships compared to the dry state (air saturated). Flooding with liquid-phase CO_2 at various pore pressures lowered velocities by approximately 8% on average compared to the air-saturated state. Attenuations increased with liquid-phase CO_2 flooding compared to the air-saturated case. Experimental data agreed with the Gassmann calculations at high effective pressures. The "critical" effective pressure, at which agreement with theory occurred, varied with sandstone type. Discrepancies are thought to be due to differing micro-crack populations in the microstructure of each sandstone type. The agreement with theory at high effective pressures is significant and gives some confidence in predicting seismic behaviour under field conditions when CO_2 is injected.

Cooperative Research Centre for Greenhouse Gas Technologies
CSIRO Petroleum
PO Box 1130 Bentley,
WA, Australia, 6102
Phone: +61 8 6436 8730
Facsimile: +61 8 6436 8555
Email: tony.siggins@csiro.au

Manuscript received 23 November, 2004.
Revised manuscript received 13 December, 2005.

INTRODUCTION

Geological sequestration of CO_2 is considered by many organisations to be a viable means of dealing with the problem of carbon dioxide generation from the burning of fossil fuels, particularly in the electrical power generating industries. The intention is to inject CO_2 into the subsurface at locations and depths associated with depleted hydrocarbon fields. In many of these fields CO_2 has existed naturally for millennia either as free gas, locked in carbonates, or dissolved in oils or brines. Provided that the existing reservoir seals remain intact, sequestration of CO_2 at depth in depleted hydrocarbon fields should present negligible risk in the near or distant future. Thus, geological sequestration can be regarded as one of the promising mitigation strategies against the negative effects of atmospheric carbon dioxide on global climate change.

Dependent on the depth of storage, CO_2 will exist in various phases: at shallow depths and at ambient temperatures carbon dioxide at pore pressures less than 6 MPa will exist in the pore space of the subsurface lithology in the gaseous phase. At greater depths, where pore pressures exceed 6 MPa, carbon dioxide will be in the liquid phase. When pore pressures are above 7.38 MPa and temperatures are above 31°C, CO_2 will be in the supercritical phase.

Currently, one of the most practical geophysical remote sensing tools for monitoring subsurface CO_2 injection is seismic imaging. This can be in the form of common depth point reflection profiling, vertical seismic profiling, cross-hole tomography, or borehole acoustic logging. Interpretation of seismic data for the quantitative measurement of the distribution and saturations of CO_2 in the subsurface requires a detailed knowledge of the effects of CO_2 as a pore fluid on the seismo-acoustic response of the reservoir rocks. This paper describes some recent experiments designed to investigate this aspect under controlled laboratory conditions, but at pressures representative of in-situ reservoir conditions.

Previous work

Literature on laboratory measurements of the effects of CO_2 on the seismic properties of reservoir rocks is relatively sparse. Wang and Nur (1989) measured ultrasonic compressional (P) and shear (S) wave velocities in seven sandstones and one unconsolidated sand saturated with hexadecane, both before and after CO_2 flooding over a range of pore pressures and at temperatures above and below the critical point.

When hydrocarbons in saturated reservoirs are displaced with CO_2 the seismic velocity behaves in a complicated manner, because above the critical pressure the density of CO_2 is similar to oil, but the bulk modulus is closer to that of a gas. Duranti et al. (2000) have shown that the interaction between the density and compressibility of the CO_2 pore fluid and the subsequent effect on the seismic properties is mostly governed by pressure conditions. Ultrasonic P-wave velocities in the CO_2 flooded sandstones cores tested by Wang and Nur (1989) showed a marked decrease in P-wave velocities (V_p) above the critical pressure as a result of

the large change in compressibility from the phase change that is not accompanied by a similar reduction in density. Wang and Nur observed that P-wave velocities decreased by between 3% and 10.9% and S-wave velocities (V_s) decreased by between 3.3% and 9.5%. Xue and Ohsumi (2004) carried out an experimental investigation of P-wave velocity and deformation in a distilled water-saturated Tako Sandstone sample with CO_2 injection. Confining pressures varied between 10 and 15 MPa while pore pressures varied between 3 and 10 MPa. They observed velocity changes of -6% from the water-saturated state with CO_2 injection and -10% with critical state CO_2 injection.

Seismic velocities and pore fluids

In porous media such as reservoir materials, seismic velocities and attenuations are influenced by the elastic moduli of the reservoir rock frame and the fluid or gas filling the pores. This is expressed formally via the Gassmann equations (Gassmann, 1951). These equations relate the saturated (undrained) bulk modulus, K^* to the drained bulk modulus, K_b. Consequently, the seismic velocities, V_p and V_s, under saturated conditions are given by the following expressions:

$$V_p = [(K^* + 4\mu/3)/\rho_{sat}]^{1/2} = [(K_b + 4\mu/3 + \alpha^2 M)/\rho_{sat}]^{1/2}, \quad (1)$$

$$V_s = [\mu^*/\rho_{sat}]^{1/2}, \quad (2)$$

where M is given by effective medium theory (Gassmann, 1951) as

$$M = 1/[\phi/K_f + (1-\phi)/K_s - K_b/K_s^2], \quad (3)$$

and saturated density, ρ_{sat} is given by

$$\rho_{sat} = \phi\rho_f + (1-\phi)\rho_s. \quad (4)$$

The subscripts f and s refer to fluid and solid, respectively; μ is the drained shear modulus, μ^* is the saturated shear modulus, ϕ is porosity, and α is the Biot-Willis coefficient. It should be noted that a condition for the Gassmann model to hold is that $\mu = \mu^*$ (Berryman, 2004).

With CO_2 as the pore fluid in porous reservoir rocks such as sandstones, the velocity response to changing pressures is complicated by the phase transitions in CO_2. Each of these is accompanied by significant changes in density, ρ_f and bulk modulus, K_f. Figure 1, from Gupta and Sass, 1999, presents the pressure–density diagram for CO_2.

EXPERIMENTAL DESCRIPTION

Three cylindrical samples of sandstone were tested under triaxial stress conditions with independent control of pore pressure. Sample dimensions were 38 mm diameter with lengths ranging from 38 mm to 76 mm. The three samples were: a synthetic sandstone sample with a calcite inter-granular cement (CIPS); a synthetic sandstone sample with a silica inter-granular cement; and a field sample from 1677 m depth from the Australian Otway Basin, C Seam, Waarre Formation. This sample, from the Boggy Creek No.1 well, was a friable coarse-grained quartzitic sandstone/mudstone with carbonaceous inclusions. Porosities were respectively: 32% for the CIPS sandstone, 33% for the silica-cemented material, and 26% for the Waarre C Seam material. The synthetic sandstones were chosen as the two manufacturing processes enable close control over the mineral content, grain size distribution, porosity, and permeability of the sandstones. The

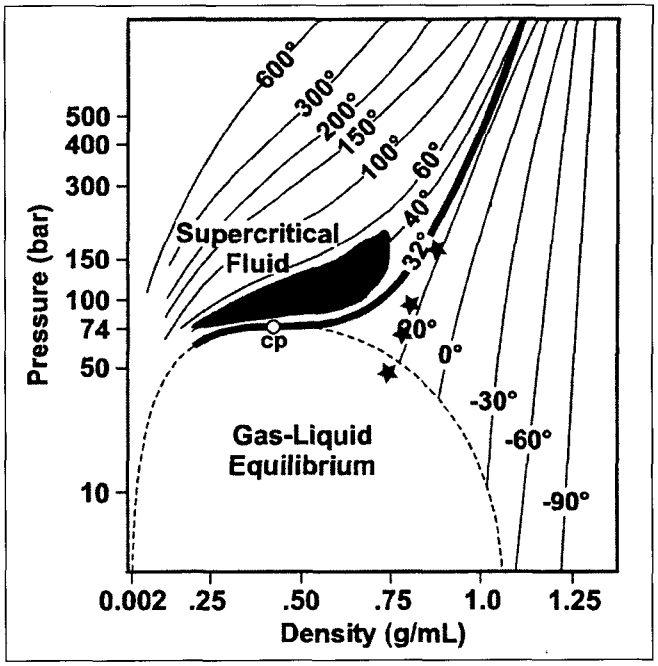

Fig. 1. Pressure – fluid density phase diagram for CO_2 (after Gupta and Sass, 1999), together with our experimental conditions (stars). 10 bar is equal to 1 MPa.

CIPS proprietary process and sandstone properties are described by Sherlock et al. (2005), and the silica cementation process is described by Wang et al. (1997).

In addition, the calcite inter-granular cement in the CIPS case may be soluble in CO_2 under certain conditions, particularly when irreducible water is present in the sandstone pore space, whereas the silica cement is not soluble. Thus the synthetic sandstones can be considered as analogues to lithologies with microstructures modified by CO_2 accumulations such as those encountered in the Otway Basin and described by Watson, 2002.

Equipment used for the sandstone testing comprises a high-stiffness load frame, a triaxial pressure cell and systems for cell and pore pressure control (Figure 2). Our triaxial rig has independent control of pore pressure, confining pressure, and axial load, to the operational upper limits of 70 MPa, 70 Mpa, and 400 MPa respectively. The inner diameter of the cell is considerably larger than the sample, allowing the installation of internal instruments such as a load cell, radial and axial displacement transducers, acoustic transducers, and temperature sensors. The sample stack assembly (Figure 3) includes:

The sandstone specimen mounted between top and base platens, encased in a flexible, impermeable Viton membrane (0.75 mm thick), separating the confining fluid from the specimen,

- Two steel loading platens housing ultrasonic P- and S-wave elements with provision for pore-pressure measurement at both ends of the specimen. Shallow grooves are engraved on the platen surfaces to distribute pore fluid evenly and allow testing without using a porous disk. The diameter of the platens is 38 mm, the same as that of the specimen (within ±0.05 mm),
- Two diametrically positioned linear variable differential transformers (LVDTs) clamped on the top and bottom platens, to measure axial displacements,
- A load cell, located underneath the bottom platen,
- An auxiliary pressure cell plumbed into the pore-pressure lines containing CO_2 as the pore fluid. The pore pressure in this case was controlled manually.

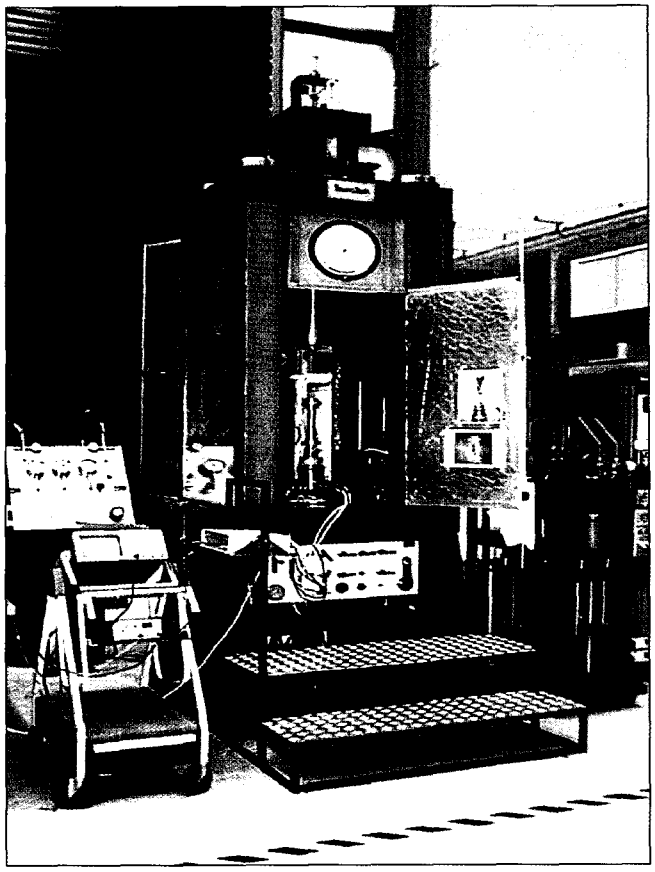

Fig. 2. Computer-controlled triaxial pressure cell with independent control of pore pressure with the pore fluid maintained in both gaseous and liquid phases as required.

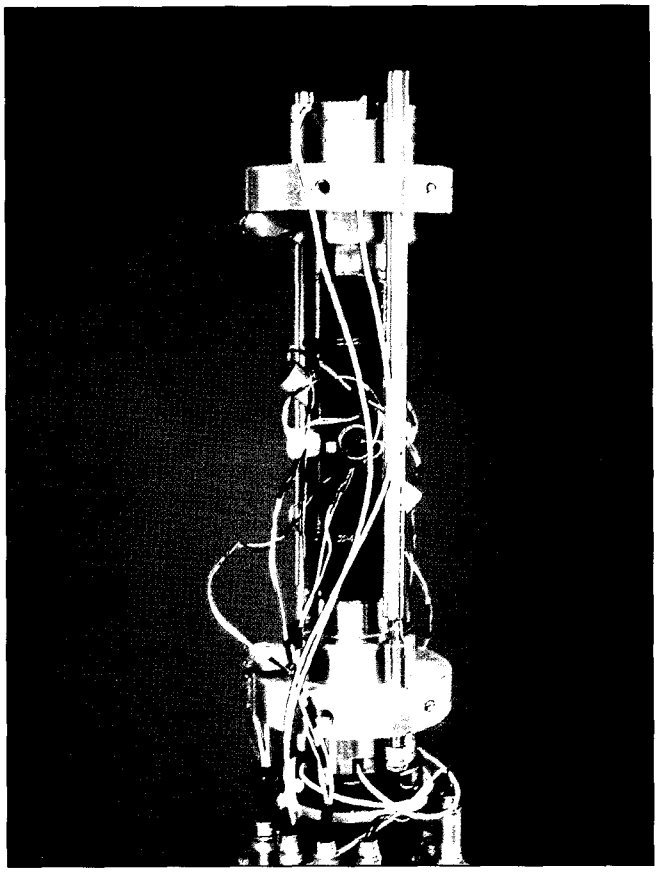

Fig. 3. Sample stack, showing sample encased in a synthetic rubber membrane (VITON), ultrasonic transducer array, and axial extensometers (LVDTs).

Samples were first tested under room-dried conditions with ambient air pore pressure and confining pressures typically ranging from 5 MPa to 60 MPa. Velocities were recorded at 5 MPa increments on both the loading and unloading cycles. CO_2 flooding of the sample in-situ was then carried out at a pore pressure of 6 MPa (CO_2 is in the gaseous phase at this pressure – refer to Figure 1a) and the loading cycles repeated. Pressure of the CO_2 in the auxiliary chamber was then increased to nominally 7 MPa where a phase transition occurred and CO_2 was in the liquid phase. The sample was then flooded with liquid phase CO_2 and loading cycles and velocity measurements repeated. Pore pressures were increased in 5 MPa steps up to 22 MPa. A check on the liquid CO_2 saturation state was provided by monitoring the increase of pore pressure in the sample (with top and bottom pore line taps closed) as confining pressure increased. Note that this increase does not occur with pore pressures in the gaseous phase. All experiments were conducted at ambient temperature which was 22±0.5°C.

RESULTS

Velocity–pore pressure response for the CIPS sandstone is presented in Figure 4, and tabulated in the Appendix in Table A1. Arrival time picks were based on first breaks estimated from approximately 1% of the first peak amplitude. Data for both the room-dried condition and the gaseous phase CO_2 saturated condition at 6 MPa pore pressure is presented in Figure 4. The velocity data is plotted against effective pressure. Effective pressure is defined as confining pressure, P_c, minus pore pressure, P_p, i.e., $P_c - P_p$. In the dry state (air saturated) the pore pressure was at atmospheric pressure. Figure 5 presents velocity versus effective pressure for the three sandstones, both dry and saturated with CO_2 in the liquid phase at 22°C and 17 MPa pore pressure. Both compressional, P-wave and shear, S-wave data is presented. Uncertainties were ±0.1 microseconds for P-wave arrival times and ±0.2 microseconds for S-waves, corresponding to velocity uncertainties of ±0.4%. For comparison, the predicted responses, calculated using effective medium theory (Gassmann, 1951), equations (1) to (4), are superimposed on these plots as solid curves. Figure 5 also presents attenuation versus effective pressure for both the dry and CO_2 fluid saturated states. Attenuation was calculated from $1/Q_p$ where Q_p was determined using a spectral ratio method, details of which are described by Töksöz et al. (1979).

DISCUSSION

Hysteresis in the velocity response with confining pressure was a significant factor in the dry samples, and made selecting the drained ("dry") state for fluid substitution calculations somewhat difficult. For example, the CIPS sandstone in the dry state showed significant hysteresis in P-wave velocity during the first loading/unloading cycle, but appeared to reach a stable state after which the V_p versus effective stress response was relatively repeatable. The return path unloading cycle velocity versus effective stress response of the dry sandstones was then used as a basis for the fluid substitution calculations. Effective medium theory requires both fluid density and fluid bulk modulus to be determined at each pore pressure, covering both liquid and gaseous regions of the CO_2 phase diagram. These densities and moduli were calculated using a software tool developed by Jonathon Ennis-King at CSIRO Petroleum, based on the equation of state for CO_2 published by Span and Wagner (1996). Equations (1) to (4) were then used to determine the theoretical V_p and V_s response to effective pressure.

A comparison between the dry state and the gaseous CO_2 saturated state for all three sandstone samples (only the CIPS

Core	Cell Pressure MPa	Pore Pressure MPa	Effective Pressure MPa	Velocity V_p m/s	Velocity V_s m/s	$1/Q_p$
CIPS air - dried	40	0	40	2342.4	1568.9	0.10
	35	0	35	2301.0	1547.3	0.07
	30	0	30	2228.4	1502.5	0.07
	25	0	25	2130.5	1449.3	0.06
	20	0	20	1993.4	1374.9	0.05
	15	0	15	1887.2	1288.3	0.05
	10	0	10	1724.0	1157.6	0.04
CIPS CO_2 gas	11	5.5	5.6	1498.1	n/a	
	16	5.8	10.2	1720.5	1159.6	
	21	5.8	15.2	1887.7	1259.1	
	26	5.6	20.4	2004.2	1375.2	
	31	5.6	25.5	2154.5	1438.5	
	36	5.7	30.3	2254.3	1532.3	
	41	5.7	35.3	2279.4	1568.8	
	46	5.8	40.2	2347.0	1596.6	
CIPS CO_2 liquid	22	17.2	4.8	1354.0	n/a	0.13
	27	16.7	10.3	1574.3	n/a	0.10
	32	17.2	14.8	1737.1	1071.7	0.09
	37	17.8	19.2	1858.2	1141.3	0.09
	42	18.4	23.6	2003.1	1248.7	0.09
	47	19	28	2089.5	1314.5	0.08
	52	19.4	32.6	2159.5	1403.3	0.08
	57	20	37	2254.1	1413.0	0.07
	57	18.2	38.8	2280.4	1447.4	
	52	17.8	34.2	2208.4	1400.0	
	47	17.2	29.8	2141.1	1329.8	
	42	17.5	24.5	1981.1	1262.4	
	37	16.9	20.1	1875.3	1156.1	
	32	16.9	15.1	1736.2	1075.6	
	27	16.8	10.2	1590.0	n/a	
	22	16.9	5.1	1385.4	n/a	
Silica cement air-dried	60	0	60	2583.2	2008.4	0.05
	55	0	55	2759.7	2035.0	0.05
	50	0	50	2917.1	2018.9	0.05
	45	0	45	3032.4	2008.4	0.06
	40	0	40	3118.7	1987.6	0.06
	35	0	35	3157.2	1972.2	0.06
	30	0	30	3237.1	1942.3	0.06
	25	0	25	3237.1	1899.0	0.07
	20	0	20	3264.7	1831.0	0.08
	15	0	15	3278.6	1759.6	0.07
	10	0	10	3264.7	1649.9	0.08
Silica cement CO_2 liquid	23	17	6	1932.7	1188.7	0.09
	28	17	11	2308.1	1370.7	0.10
	33	17	16	2504.4	1456.5	0.09
	38	17	21	2642.5	1670.5	0.08
	43	17	26	2776.6	1730.6	0.08
	48	17	31	2848.6	1770.4	0.07
	53	17	36	2913.3	1803.5	0.07
	58	17	41	2992.9	1842.3	0.06
	63	17	46	3064.6	1873.6	0.06
	68	17	51	3101.4	1887.1	0.06
	58	17	41	3016.1	1837.5	
	48	17	31	2858.4	1765.7	
	38	17	21	2641.4	1666.1	
	28	17	11	2348.6	1283.6	
Waarre C seam air-dried	5	0	5	2490.4	1178.8	0.22
	10	0	10	2873.5	1248.9	0.17
	15	0	15	3056.4	1312.3	0.17
	20	0	20	3171.7	1343.8	0.17
	25	0	25	3264.1	1638.4	0.15
Waarre C seam CO_2 liquid	23	17	6	2821.1	1082.0	0.32
	28	17	11	3014.7	1155.1	0.28
	33	17	16	3106.1	1195.6	0.27
	38	17	21	3203.1	1214.5	0.25
	43	17	26	3271.3	1243.9	0.24
	45	17	28	3306.5	1238.9	

Table A1. Tabulation of confining pressures, pore pressures, P-wave and S-wave velocities, and attenuations.

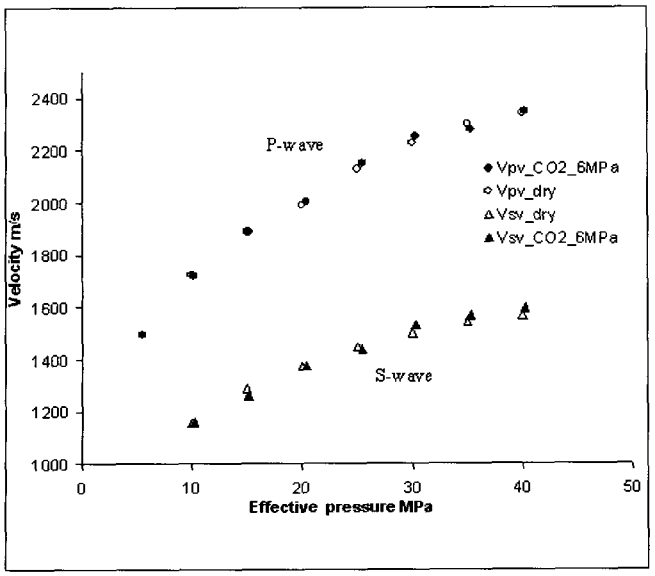

Fig. 4. Comparison of the velocity versus effective pressure response for CIPS synthetic sandstone in the room-dried state with the CO_2 saturated state. CO_2 is in the gaseous phase at a temperature of 22°C and a pore pressure of 6 MPa.

sandstone data is shown) showed little difference apart from experimental repeatability variations – Figure 4 is a typical example. This is to be expected from Gassmann theory, as the bulk modulus and density of the gas are small fractions of the sandstone frame modulus and density. Note that the pore pressure change from atmospheric to 6 MPa in this case is almost exactly balanced by an increase of 6 MPa in confining pressure. Thus the controlling variable for velocity variation is effective pressure.

With the liquid-phase CO_2 saturant there were velocity reductions of approximately 8% from the dry state in all sandstones except the Waarre field sample (where only the shear velocities changed noticeably), due mainly to the density change associated with the CO_2 phase change. The bulk modulus and density changes of the CO_2 at 22°C as the pore pressure changes from 6 MPa pore pressure to 17 MPa are respectively: 7.9×10^6 MPa to 3.0×10^8 Mpa, and 210 $kg.m^{-3}$ to 908 $kg.m^{-3}$.

The agreement between the experimental velocities for the synthetic sandstones under liquid-saturated conditions with the Gassmann predictions was particularly good at high effective pressures. In the case of the silica-cemented sandstone, agreement was excellent at effective pressures of 20 MPa and beyond. The CIPS material required effective pressures of 27 MPa and higher before agreement between experiment and theory was reached. These discrepancies are no doubt due to varying populations of high-aspect-ratio pore space (cracks and intergranular separations) in the rock structure. The solubility of the calcite intergranular cement in the CIPS material in CO_2 if some water is present (Gupta and Sass, 1999) may contribute to the formation of high-aspect-ratio pore space. Gassmann theory does not take the high compliance pore space into consideration. With the Waarre Formation sandstone the discrepancy between theory and experiment was noticeable. In this sandstone the core material had been retrieved from depth so significant damage from stress relief is to be expected. The high attenuation – more than twice that of the synthetic materials – is evidence of this damage. Microstructural damage may have compromised the structural integrity of the core sample and

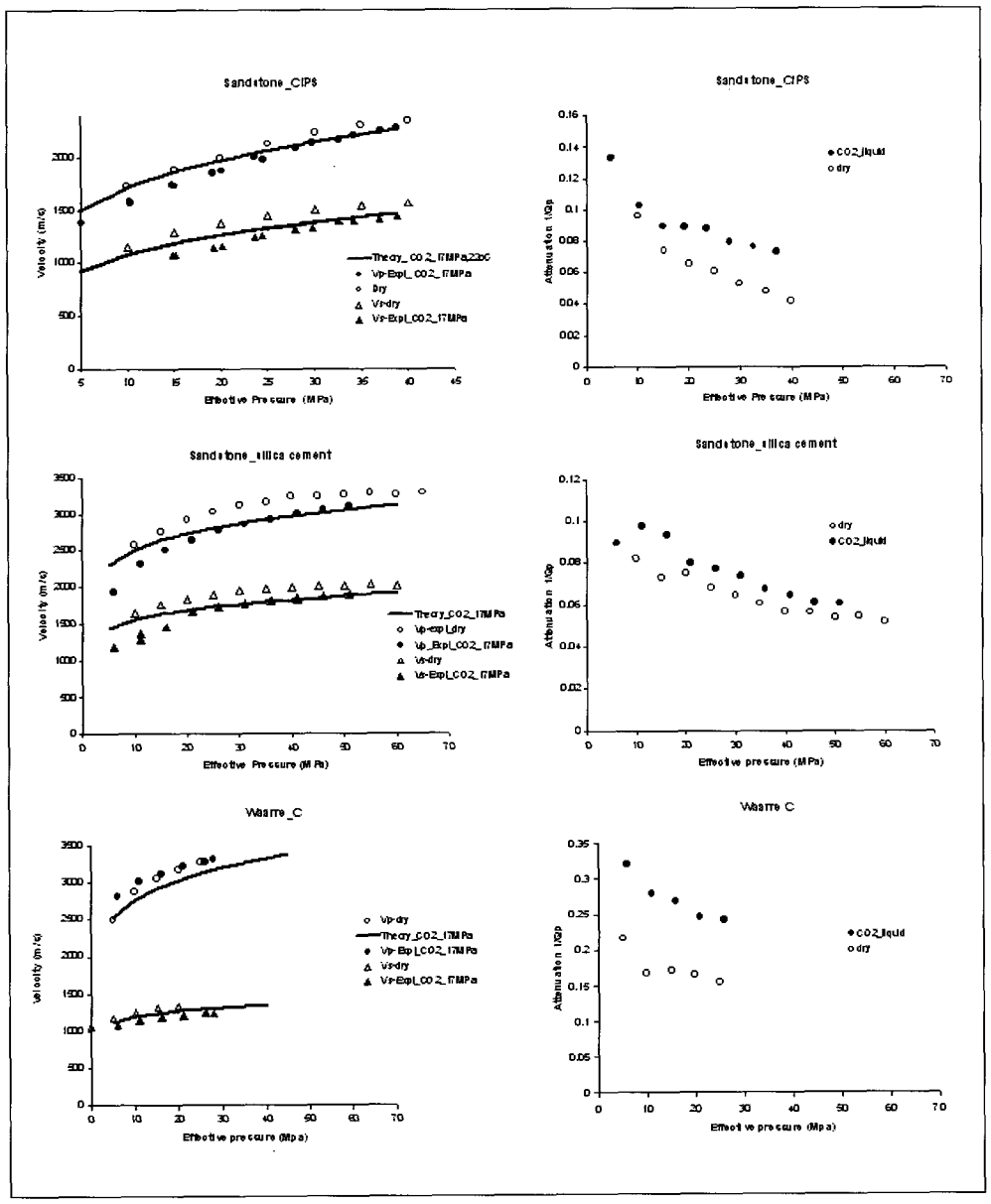

Fig. 5. Velocity versus effective pressure response in three sandstones for both dry (air saturated) and liquid CO_2 saturated conditions. Corresponding intrinsic attenuations ($1/Q_p$) are also presented. In these data CO_2 is in the liquid state at a temperature of 22°C and a pore pressure of 17 MPa. The theoretical Gassmann predictions for the liquid CO_2 saturated state for both P- and S-waves are included as solid curves.

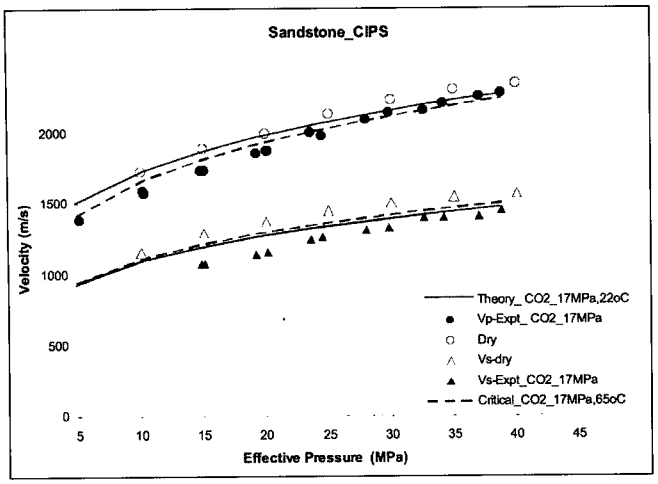

Fig. 6. Velocity–effective pressure data from an experiment on the CIPS synthetic sandstone. Dry core data is presented together with the liquid saturated CO_2 response with the CO_2 at a pore pressure of 17 MPa at a temperature of 22°C. For comparison the theoretical response using Gassmann theory is shown as a solid curve together with the expected behaviour with CO_2 in the "super-critical" phase at a pore pressure of 17 MPa at a temperature of 65°C – dashed curve.

contributed to the lack of sensitivity of the P-wave velocity to CO_2 saturation. Extrapolation of the velocity versus effective stress data trend in the Waarre Formation sample indicates that effective pressures of ~40 MPa are required before agreement with the Gassmann predictions is reached.

Critical state CO_2

Figure 6 displays again the CIPS sample data, including the computed responses (solid lines), with liquid CO_2 at 17 MPa and 22°C as the pore fluid. However, additional theoretical responses have been included for comparison. Theoretical curves (dashed lines) have been computed from the dry velocity data with CO_2 in the "super-critical" state at 17 MPa and 65°C substituted as the pore fluid. There is a further reduction in P-wave velocity, mainly due to the lower bulk modulus, 6.97×10^7 MPa, of the super-critical fluid while density decreases to 623 kg.m^{-3}. There is only a small change in the S-wave response amounting to a slight increase due to the density reduction.

CONCLUSIONS

Compared to the dry unsaturated state, both P-wave and S-wave velocities decreased in all synthetic sandstones with the addition of liquid CO_2 in the saturated state. On average, this decrease was of the order of ~8%, although the reduction in velocity varied slightly with effective pressure.

Intrinsic attenuations ($1/Q_p$) in all sandstones increased with liquid phase CO_2 saturation.

There was good agreement between the experimental results and the Gassmann predictions for the synthetic materials, particularly at effective pressures exceeding 30 MPa. Effective pressures at sequestration sites in the field are expected to be of the order of 25 MPa.

At low effective pressures, velocities were lower than the Gassmann predictions in all cases. This is thought to be due to the presence of both compliant porosity (high-aspect-ratio cracks) and less-compliant or "equant" porosity contributions to the sandstone microstructure. This departure was more pronounced in the calcite-cemented sandstone, possibly because of the solubility of the calcite cement in CO_2 with some small amounts of water present. (Samples were air-dried at room temperature).

The Waarre Formation C Seam core sample showed poorer agreement with Gassmann predictions than the synthetic samples. Attenuations were also very high (more than twice that of the other samples). This is considered to result from the presence of considerable damage (cracks), possibly due to stress relief during coring. Possible breakdown of the carbonaceous elements in the microstructure during the testing may also be a contributing factor.

These results should be a useful guide for interpreting the response of time-lapse seismic monitoring of similar sandstone formations following CO_2 injection at depth. In particular, the experiments and theory indicate that the change in P-wave velocity with CO_2 in the liquid phase to the supercritical phase will be difficult to distinguish.

ACKNOWLEDGMENTS

This work was carried out with support from the Cooperative Research Centre for Greenhouse Gas Technologies, Storage Program under the Monitoring and Verification Project. The author thanks his colleagues David Dewhurst, Craig Harbers, and Kevin Dodds for support during these experiments.

REFERENCES

Berryman J.G., 1999, Origin of Gassmann's equation: *Geophysics*, **64**, 1627–1629.

Duranti, L., Davis, T. L., and Benson, R.D., 2000, Time-lapse analysis and detection of fluid changes at Vacuum Field, New Mexico: *70th Annual International Meeting, Society of Exploration Geophysicists, Extended Abstracts*, 1528–1531.

Gassmann F., 1951, Über die Elastizität poröser Medien: *Vierteljahrsschrift der Naturforschenden Gesellschaft in Zürich*, **96**, 1–23.

Gupta, N., and Sass, B., 1999, *Hydrodynamic and geochemical modeling for carbon dioxide sequestration in deep saline formations, Final Report, 28 February 1999: DE-AF26-98FT00874*: Report to US Department of Energy (DOE), Federal Energy Technology Center.

Sherlock, D.H., Scoby-Smith, L., and Montague, E., 2005, Time-lapse analogue reservoir modelling of turbidite channel sands: *Exploration Geophysics*, **36**, 216–223.

Span, R., and Wagner, W., 1996, A new equation of state for Carbon Dioxide covering the fluid region from the Triple-Point temperature to 1100 K at pressures up to 800 Mpa: *Journal of Physical and Chemical Reference Data*, **25**, 1509–1596.

Töksöz, M.N., Johnston, D.H., and Timur, A., 1979, Attenuation of seismic waves in dry and saturated rocks. 1, Laboratory measurements: *Geophysics*, **44**, 681–690.

Wang, Z., and Nur, A.M., 1989, Effects of CO_2 flooding on wave velocities in rocks with hydrocarbons: SPE Reservoir Engineering, **4**, 429–436.

Wang, D.F., Yassir, N., Enever, J., and Davies, P., 1997, Laboratory investigation of core-based stress measurement using synthetic sandstone: *International Journal of Rock Mechanics and Mining Sciences & Geomechanics Abstracts*, **34**, 654.

Watson, M.N., Zwingmann, N., and Lemon, N.M., 2004, The Ladbroke Grove-Katnook Carbon Dioxide Natural Laboratory: A Recent C02 Accumulation in a Lithic Sandstone Reservoir: *Energy*, **29**, 1457–1466.

Xue, Z., and Ohsumi, T., 2004, Seismic monitoring of CO_2 migration in water-saturated porous sandstone: *Exploration Geophysics*, **35**, 25–32.

CO_2で飽和した砂岩の速度ー有効応力応答

アンソニー F シギンス[1]

要 旨： 3つの異なった砂岩(合成サンプル2個と現位置サンプル1個)を、原位置での典型的な封圧および貯留層圧条件下において、超音波を用いた計測を行った。これらの砂岩は: CSIRO Calcite In-situ Precipitation Process(CIPS)を使って作った2種類の合成砂岩（粒子間セメントが方解石と珪石の2種類)、および、CO_2圧入パイロットプロジェクトのターゲット貯留岩である Otway Basin の Boggy Creek-1 号井の Waarre Formation から取得されたコアサンプルの3種である。初期テストは室内乾燥したコアで 5MPa のステップにごとに 65MPa までの封圧を変化させて行われた。続いて、コアを 22℃,6MPa の気相 CO_2 で充填したうえで、7MPa から 17MPa まで 5MPa 間隔で圧力を変化させながら、22℃の液相 CO_2 を圧入した。封圧は 10MPa から 65MPa まで変化させた。P 波と S 波の両方の超音波波形は各々の有効圧力増加ごとに記録され、各々について、速度対有効圧力応答の計算を行った。減衰(1/Qp)は、波形データからスペクトル比法で計算された。各砂岩の（有効圧力の関数である）速度の理論計算は、CO2 圧力ー密度、CO2 の体積弾性率ー圧力フェーズダイヤグラム、および Gassmann の有効媒体(effective medium)理論を使用して行なった。

気相 CO_2 でコアを飽和した場合と、乾燥状態下(空気で飽和した状態)とを比べると、速度 - 有効応力関係における変化は無視できるほど些少である。孔隙圧を変化させて液相 CO_2 で飽和した場合、空気で飽和した状態と的に比べて、速度は平均して約 8%減少した。振幅の減衰は液相 CO_2 飽和の場合の方が、空気飽和の場合と比較して大きかった。実験データは高い有効圧力下では Gassmann 法による計算と整合する。

理論と整合し始める”臨界”有効圧力値は、砂岩のタイプごとに異なることがわかった。この違いは、それぞれの砂岩タイプの微小構造中の、微小クラック数の違いに起因すると考えられる。高い有効圧力下での理論との一致は意義が大きい、なぜならば、現場条件下で CO_2 圧入が行われた場合の地震波の挙動を、より高い信頼度で予測することが可能になるためである。

キーワード： CO_2、地層処分、孔隙内圧力、速度、減衰

CO_2로 포화된 사암의 속도-유효응력 반응

Anthony F. Siggins[1]

요 약： 세 개의 서로 다른 사암 샘플들 -두 개의 합성 샘플과 한 개의 현장 샘플- 에 대해 현장 저류층의 대표적인 구속압력과 공극압력하에서 초음파 시험이 수행되었다. 세가지 사암 샘플들은 (a) 캘사이트 시멘트(calcite intergranular cement (CIPS))로 만든 합성사암, (b) 실리카 시멘트(silica intergranular cement)로 만든 합성 사암 (c) Otway Basin 의 Boggy Creek 1 시추공에서 시도되는 CO_2 파일럿 프로젝트의 대상 암석층 중 Waarre 층으로부터 추출한 코아 샘플로 구성되어 있다. 공극률은 각각 32%, 33%, 26%이다. 초기시험은 실내건조(room-dried) 상태에 있는 코아들에 대해 구속응력을 5 MPa 씩 단계별로 65 MPa 까지 증가시키며 이루어졌다. 그리고 나서 모든 코아들에 처음에는 온도 22°C 에서 6 MPa 공극압력으로 기체상의 CO_2 를, 그 다음에는 온도 22°C 에서 7 MPa 부터 17 MPa 까지 5 MPa 씩 증가시키면서 액체상의 CO_2 를 주입하였다. 구속응력은 10 MPa 부터 65 MPa 까지 달리 하였다. P 와 S 초음파 파형들이 유효응력이 증가할 때마다 기록되었다. 속도-유효응력 반응들이 P 파와 S 파에 대해 실험 자료들로부터 계산되었으며, 감쇠(1/Qp)들은 스펙트럼 비 방법을 이용하여 파형들로부터 계산되었다. 각각의 사암들에 대한 이론적인 속도-유효응력 계산은 CO_2 압력-밀도 와 CO_2 체적계수-압력 상 다이어그램(phase diagram), Gassmann 유효 매질 이론(effective medium theory)을 이용하여 구하였다.
기체상의 CO_2 주입은 속도-유효응력에서 건조상태(공기로 포화된 상태)에 비해 거의 무시할만한 변화를 가져왔다. 다양한 공극압력에서 액체상의 CO_2 주입은 공기로 포화된 상태에 비해 속도-유효응력 반응을 평균 약 8% 정도 낮게 한다. 실험자료들은 높은 유효응력에서 Gassmann 계산들과 일치한다. 이러한 이론과 일치하는 “임계” 유효응력은 사암의 종류에 따라 달라진다. 이 차이는 각각의 사암 종류의 미세구조에서 미세 균열 수의 차이에 기인한 것이라 생각된다. 높은 유효응력에서의 이론과 의미있게 일치하였으며, CO_2 주입 시 현장에서의 탄성파 거동을 예상하는데 있어서 어느 정도 확신을 준다.

주요어： 이산화탄소, 격리, 공극압력, 속도, 감쇠

温暖化ガス技術共同研究センター
1 オーストラリア連邦科学産業研究機構
CSIRO Petroleum, PO Box 1130, BLENTY, WA, Australia 6102

Cooperative Research Centre for Greenhouse Gas Technologies
1 CSIRO Petroleum